Pergamon

Acta mater. 49 (2001) 2625–2634

Acta MATERIALIA

www.elsevier.com/locate/actamat

INTERACTION OF HYDROGEN AND DEUTERIUM WITH DISLOCATIONS IN PALLADIUM AS OBSERVED BY SMALL ANGLE NEUTRON SCATTERING

M. MAXELON[1], A. PUNDT[1], W. PYCKHOUT-HINTZEN[2], J. BARKER[3] and R. KIRCHHEIM[1]†

[1]Der Georg-August-Universität Göttingen, Institut für Materialphysik, Hospitalstrasse 3-7, D-37073 Göttingen, Germany, [2]FZ Jülich, Institut für Festkörperforschung, Germany and [3]NIST, Center for Neutron Research, NIST, Gaithersburg, USA

(Received 20 February 2001; received in revised form 3 May 2001; accepted 4 May 2001)

Abstract—Small angle neutron scattering (SANS) measurements on Pd samples containing dislocations with a density of a few 10^{11} cm^{-2} reveal an additional intensity for a scattering vector of 0.02 Å^{-1} to 0.2 Å^{-1} after loading with hydrogen (H) or deuterium (D). The corresponding net cross section is inversely proportional to the scattering vector as expected for line type scattering objects with a superimposed exponential decrease stemming from scattering within the Guinier-regime. This experimental finding is in accordance with a model where extended segregation of H or D within the dilated regions of edge dislocations occurs. In a first order approximation this corresponds to a precipitation of cylindrically shaped hydrides along the dislocation line and can be treated quantitatively yielding radii in agreement with SANS data. Whereas gas volumetric measurements at the same total concentration reveal no difference for the amount of H- and D-segregation, there is a pronounced effective difference in SANS intensities which cannot be explained by the different scattering lengths alone. However, the different sign of the latter quantity in combinations with an expected volume expansion within the hydride/deuteride region provides a reasonable explanation of the intensity difference observed. Knowing the amount of segregated H or D from gas volumetry and the dislocation density from electron microscopy the SANS results can be explained in a self consistent way.

Keywords: Neutron scattering; Dislocations; Portevin–Le Chatalier effect; Segregation; Hydrogen in metals

1. INTRODUCTION

Since the pioneering work by Cottrell [1] it has been generally accepted that solute atoms segregate at dislocations due to the elastic interaction between the strain field around a solute atom and the stress field of a dislocation. The local segregation at dislocations or the so-called Cottrell cloud reduces the mobility of dislocations and, therefore, affects the plastic deformation of metals. The dynamics of this interaction for instance gives rise to serrated yielding.

In this paper we will consider the static case only and for interstitial solutes the situation is simplified by the fact that they have a strong dilatational strain field which gives rise to a strong interaction with edge dislocations. Compared to carbon in α-Fe where a tetragonal distortion of the lattice leads to an attractive interaction with screw dislocations, hydrogen atoms do not interact with these dislocations in fcc-Pd, because H-atoms occupy octahedral sites in this metal with a strain field of cubic symmetry. As the trace of the strain tensor corresponds to the partial molar volume of hydrogen V_H and the trace of the stress tensor of an edge dislocation is one third of the hydrostatic pressure $p(\vec{r},\theta)$, the elastic interaction energy is

$$W_{el} = V_H p(\vec{r},\theta), \tag{1}$$

where $\vec{r},\theta$ are cylindrical coordinates (cf. Fig. 1). Calculating the stress field around an edge dislocation [2] gives

$$p(\vec{r},\theta) = \frac{Gb(1+\nu)}{3\pi(1-\nu)} \frac{\sin\theta}{|\vec{r}|}, \tag{2}$$

† To whom all correspondence should be addressed. Tel.: +49-551-39-5001; fax: +49-551-39-5012.
E-mail address: rkirch@umpa03.gwdg.de (R. Kirchheim)

1359-6454/01/$20.00
PII: S1359-6454(01)00185-9

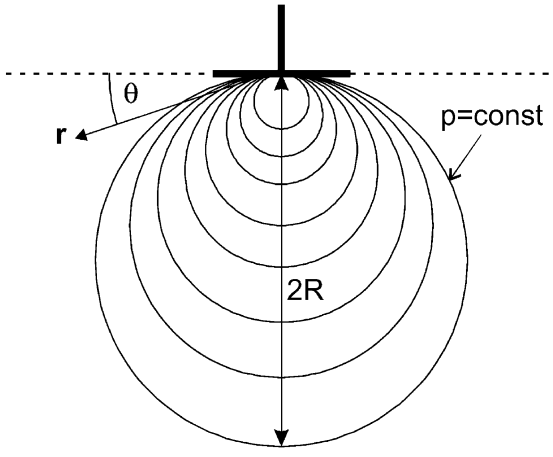

Fig. 1. Cylindrical coordinates with the origin at the dislocation core, glide plane (dashed line) and circle (cylinder in 3 dimensions) of constant hydrostatic stress.

where G is the shear modulus, b the Burgers vector and ν the Poisson's ratio. Isobaric surfaces correspond to cylinders with the glide plane as a tangential plane. In the 2-dimensional cross section in Fig. 1, isobars correspond to circles and the pressure on these circles can be expressed by the radius R as

$$p(R,\theta) = \frac{Gb(1+\nu)}{3\pi(1-\nu)}\frac{1}{2R}. \qquad (3)$$

The equations presented so far are based on continuum theories neglecting the discrete nature of the metal lattice. As a consequence, p approaches infinity in the dislocation core, i.e. for $R \rightarrow 0$, and applying Boltzmann Statistics in order to calculate the occupancy in the stress field [3] leads to infinite local concentrations in the core. These problems can be circumvented by using an inner cut-off radius [2] and by applying Fermi-Dirac Statistics [4, 5, 6]. In the present study H-concentrations are always so large that the dislocation core is saturated and has not been taken into account.

Usually segregation of solute atoms at dislocations is observed experimentally in an indirect way by either studying the effect of a reduced dislocation mobility [7: p. 191] or by the reduction of both solute activity and mobility [6]. In those cases where an extended segregation exists, direct observation within an electron microscope becomes possible [8, 9]. With the exceptional spatial resolution and high elemental sensitivity of the tomographic atom probe, segregation of boron to an edge dislocation has recently been revealed in three dimensions [10].

A somewhat different approach to determine segregation of deuterium to dislocations is small angle neutron scattering (SANS), which has been applied to the Pd-D and V-D system by various groups [11, 12, 13, 14]. In contrast with the microscopic technique, where only one or a few dislocations can be studied, SANS averages over a large volume. In addition it is very difficult to study solute segregation by TEM in a region of less than 1 nm and for a solute like hydrogen, analytical tools as EDX and EELS are not applicable. Hydrogen may also escape into the vacuum or may be absorbed from the residual gases depending on the partial pressure of the metal–hydrogen system under investigation. Using the tomographic atom probe allows hydrogen to be detected but the analysis has to be done at very low temperatures around 50 K where most of the hydrogen is precipitated as a hydride. SANS measurements can be done over a large range of temperatures and partial pressures of hydrogen and, therefore, thermodynamic equilibrium, will be established. However, the interpretation of SANS-data requires an assumption or estimation of the local deuterium distribution around the dislocation. The different procedures used in this context are discussed in this study also. However, the main purpose of the present study is to provide experimental results for SANS on both H- and D-segregation at dislocations. The different sign of the scattering length of neutrons for hydrogen and deuterium atoms provides new insight into the interaction with dislocations. In addition, a systematic study of the concentration dependence of segregation was conducted for the first time.

2. EXPECTED SCATTERING LAWS

The scattered intensity is usually expressed by the macroscopic scattering cross section $d\Sigma/d\Omega$ which can be given in cylindrical coordinates as

$$\frac{d\Sigma}{d\Omega} = N_e\langle\left|\int \Delta\rho(r,z,\theta)\exp(i\vec{Q}\vec{r})d^3\vec{r}\right|^2\rangle, \qquad (4)$$

where N_e is the number of scattering entities, $\Delta\rho$ the difference in scattering length density, i.e. number of scattering atoms times their scattering length b_n per unit volume, and $\vec{Q}$ is the scattering vector. Brackets correspond to averaging over various directions of oriented scattering units, i.e. dislocation lines. An evaluation of equation 4 for scattering cylinders is given in Appendix A.

As we have to compare SANS from bare dislocations with those decorated with either H- or D-atoms, we will consider the effect of the bare dislocations first. Scattering by edge dislocations without segregated solute atoms was treated by Atkinson and Hirsch [16] yielding for the dislocation core

$$\frac{d\Sigma}{d\Omega} = N_d\frac{2\pi H(\pi r_c^2)^2\Delta\rho^2}{Q} = N_d\frac{2\pi H(\pi r_c^2)^2}{Q}\left(\frac{b_n\Delta V}{\Omega V}\right)^2, \qquad (5)$$

where N_d is the number of dislocation lines per unit volume, H half of their length, r_c the radius of the

dislocation core, $\Delta V/V$ is the relative decrease of atomic density within the dislocation core, Ω is the atomic volume, and Q is the magnitude of the scattering vector. The definition of the scattering vector Q for neutron scattering is different to the one used for X-rays with $s = 2\cdot\sin(\theta/2)/\lambda$ (θ being the scattering angle) and, therefore, $Q = 2\pi s$ has been used for a comparison with the results of Atkinson and Hirsch [16]. Equation 5 is equivalent with scattering from randomly oriented cylinders of length $2H$ and radius r_c with a decreased scattering length density due to the lower atomic density in the core (cf. Appendix A).

Scattering by the strain field of an edge dislocation has a much stronger Q-dependence which can be expressed by [16]:

$$\frac{d\Sigma}{d\Omega} = \frac{2N_d H F^2 \pi^2 4\pi b_n^2}{2\Omega^2 \Omega^3} \text{ with } F = \frac{b}{2\pi}\frac{1-2\nu}{1-\nu}, \qquad (6)$$

where b is the Burgers vector which has to be distinguished from the scattering length b_n. The contribution from screw dislocations is less pronounced [16] and will be disregarded in the following. The Q^{-3} power law was verified by small angle X-ray scattering for high purity and deformed aluminum [17].

By decorating the dislocation with hydrogen or deuterium, an additional term has to be included in the contrast $\Delta\rho$, i.e. the difference of the scattering length density between the strain of a dislocation and the perfect crystal of the metal. If a net cross section is calculated according to the definition

$$\left(\frac{d\Sigma}{d\Omega}\right)_{\text{net}} = \left(\frac{d\Sigma}{d\Omega}\right)_{c_H} - \left(\frac{d\Sigma}{d\Omega}\right)_{0{,}0\%-H} \qquad (7)$$

as the difference between a sample containing hydrogen (deuterium) and one without hydrogen (deuterium), it always contains a mixed term. This mixed term being a product of the contribution from the dislocation and the one from the solute atoms arises because of the squared term in equation 4. This has been discussed by Ross and Stefanopoulus [14] in detail. As the scattering length of H and D have different signs the mixed term has a different sign for the two isotopes as well. Of course this is true for other mixed terms as well, arising from the interaction of the isotopes with other defects.

It will be shown later that the contribution from the dislocations to the total scattering cross section is small compared to the contributions from both H and D and, therefore, the mixed term is considered not to contribute much to the net cross section. Thus the net cross section is assumed to describe the effect of the H- and D-distribution only. The spatial distribution of solute atoms around a dislocation can be described in the framework of an elastic interaction and Fermi-Dirac Statistics [4, 5, 11, 14] leading to a non-homogeneous segregation where the H-concentration decreases with increasing distance from the dislocation core. This is difficult to be included in equation 4 and requires numerical integration [14]. The situation is even more complex if local volume changes associated with the incorporation of H-atoms affect the scattering length density of the metal atoms and/or if local H-concentrations become so large that H-H interaction plays an important role. There is evidence from measurements of the chemical potential of H, resistivity increment, etc. [6, 11], that there is a pronounced segregation of H at dislocations which can be described as a hydride formation. Neglecting coherency stresses, the isobaric surfaces arising from the stress field of an edge dislocation are cylinders and, therefore, the interaction energy (cf. equation 1) and the chemical potential of H have to be constant on these surfaces as well. As a result the hydrides have to be of cylindrical geometry. Thus it is justified to consider the scattering from randomly oriented cylinders in a first order approximation and compare it with experimental results. It is shown in Appendix A that for this case equation 4 yields

$$\frac{d\Sigma}{d\Omega} = \frac{2\pi^3 N_d H R_0^4 \Delta\rho^2}{Q}\exp\left[-\frac{1}{4}Q^2R_0^2\right], \qquad (8)$$

where R_0 is the radius of the cylinder and per definition of H and N_d the product $2HN_d$ corresponds to the dislocation density. The scattering contrast of the hydride cylinders of composition PdH_α is given by

$$\Delta\rho = \frac{b_{Pd}}{f\Omega} + \alpha\frac{b_H}{\Omega} - \frac{b_{Pd}}{\Omega}, \qquad (9)$$

where Ω is the atomic volume of Pd, b_H and b_{Pd} are the coherent scattering lengths of Pd and H and $f>1$ describes a volume increase due to hydride formation, which is 1.12 for the unconstrained formation of the β-phase of $PdH_{0.6}$ [18]. With tabulated values of b [19] equation 9 becomes

$$\Delta\rho = 4\cdot10^{10}\cdot\frac{1-f}{f} + \alpha\cdot\begin{cases} -2.53\cdot10^{10} & \text{for H} \\ 4.52\cdot10^{10} & \text{for D} \end{cases}. \qquad (10)$$

As the first term on the right hand side of equation 10 is negative, the volume expansion caused by segregated hydrogen increases the absolute value of the contrast and vice versa for deuterium. The stronger coherent scattering of deuterium compared to hydrogen is then compensated to a large extent by the volume expansion.

3. EXPERIMENTAL PROCEDURE

3.1. Sample preparation and characterization

Palladium was used as cold rolled sheets of 1 mm thickness and 99.95% purity containing about $1.1 \cdot 10^{-4}$ atomic fractions of oxygen and $2.0 \cdot 10^{-4}$ of carbon. The samples were annealed in vacuum at 1150°C and some of them were loaded with hydrogen in 0.5 molar sulfuric acid by a constant cathodic current of 20 mA/cm^2 for about one day which leads to the formation of the β-phase corresponding to a concentration of 0.73 H/Pd which was determined by weighing. Hydrogen was then removed by anodic polarization at 0.8 V (versus a saturated calomel electrode). By this procedure, the two-phase field in the Pd-H phase diagram is passed twice. It is well known that *both* the formation of the β-phase with a volume misfit of about 12% [18] during loading *and* the formation of the α-phase (-12% misfit) during unloading leads to the formation of rather uniformly distributed dislocations, which are preferentially edge type ones [20]. This was confirmed by our own electron microscopy observations, which yielded a dislocation density of 10^8 cm^{-2} for the annealed samples and about $1 \cdot 10^{11}$ to $2 \cdot 10^{11}$ cm^{-2} for the cycled sample, i.e. the ones which experienced an excursion into the β-phase. There are a number of systematic errors involved in determining dislocation densities by TEM, as some dislocations may leave the sample during thinning, some may not show a contrast during imaging, and the densities may vary from one viewing area to another one. In comparison to a cold rolled sample, the cycled ones did not contain cell walls of agglomerated dislocations. In order to increase the dislocation density further we cycled the cold rolled samples without annealing.

Doping the SANS samples with certain amounts of H or D was done electrochemically at room temperature in 0.5M H_2SO_4 in H_2O or 0.5M D_2SO_4 in D_2O, respectively, where the amount of H or D can be calculated from the electric charge by Faraday's Law. Current densities were below 0.3 mA/cm^2 to warrant 100% current yields [6]. After rinsing and drying, the samples were encapsulated in a silica tube for neutron scattering measurements. H- or D-losses occurring by desorption during the transfer of the samples from the electrolyte into the SANS sample holder or by building up the equilibrium pressure within the evacuated sample holder were negligible. These losses were calculated by assuming the worst condition of zero concentration on the sample surface and solving Fick's Second Law. In one case samples were doped by absorbing either H or D from the gas phase at 80°C, where the concentration was determined from the pressure drop in a closed system. In this case the samples were placed in a circular hole of an aluminium sheet. To seal the samples from hydrogen losses, sapphire windows were glued to both sides of the plate. Estimations of these losses were found to be negligible, assuming (i) a maximum desorption rate by diffusion without surface barriers during sample transfer, (ii) a filling of the small volume in between the sapphire windows (<1 mm^3) up to the equilibrium partial pressure and (iii) the formation of water from the enclosed oxygen.

3.2. SANS measurements

Most of the SANS measurements were performed at the Forschungszentrum Jülich, Germany, using the small angle diffractometer KWS1. The distance between sample and detector was chosen to be 1.25 m, 2 m and 8 m in order to cover the range of $Q = 0.005$Å^{-1} to 0.25 Å^{-1}. The scattering data were calibrated using the incoherent scattering from a secondary Lupolen standard. The following equation was used to calculate the scattering cross section $d\Sigma/d\Omega$ from the measured intensities I:

$$\frac{d\Sigma}{d\Omega} = \frac{T_{\text{std}} D_{\text{std}} A_{\text{std}} \left(\frac{d\Sigma}{d\Omega}\right)_{\text{std}} L^2_{\text{sample}}}{T_{\text{sample + cell}} D_{\text{sample}} A_{\text{sample}} L^2_{\text{std}} \langle I \rangle_{\text{std}}} \cdot [I_{\text{sample + cell}} - I_{\text{background}} - T_{\text{sample}} \cdot (I_{\text{cell}} + I_{\text{background}})], \tag{11}$$

where the index "std" refers to Lupolen as the calibration standard, T is the transmission of the sample, D its thickness, A the area of the beam and L the distance between sample and detector.

In addition, a few measurements were performed at the National Institute of Standards and Technology, Gaithersburg, MD at the NG-7 30 m small angle scattering instrument with $Q = 2.5 \cdot 10^{-3}$ Å^{-1} to 0.5 Å^{-1}, using the gas-doped samples and silica glass as a standard.

There was no anisotropy in the scattering signals. Therefore, we took the radial mean value and subtracted the incoherent contribution mainly arising from hydrogen. Results with a low statistical error were obtained from samples charged with hydrogen despite its strong incoherent scattering. Because of its smaller incoherent and its larger coherent scattering cross section, deuterium is the natural choice for studying interactions of hydrogen isotopes with dislocations. However, as discussed previously, the expansion of the lattice by hydrogen is advantageous.

3.3. Gas volumetry

Metals with a high dislocation density absorb more hydrogen than well annealed samples for the same partial pressure of hydrogen because of the attractive interaction between the dislocations and dissolved hydrogen atoms. This effect has been well studied for Palladium [6, 11, 21] and the solubility enhancement is of the order of 20% for the concentration range of 0.1 to 1 at.-% H. Using the samples of this study, measurements were performed at 80°C in order to accelerate hydrogen up-take. Thus a sample annealed at 1150°C for 2 h in a vacuum furnace was transformed into the β-phase at 80°C by exposing the sample

to a hydrogen pressure of 700 mbar. The hydrogen was removed by evacuating. By this excursion to the β-phase, dislocations are produced with a density being determined by the former total hydrogen content [22] and the kinetics of the hydrogen up-take. As the samples used for SANS measurements were charged faster and to a higher total hydrogen content by using an electrochemical process, they are assumed to have a higher dislocation density compared to those who were exposed to gaseous hydrogen.

4. RESULTS

4.1. Background intensity

As can be seen in Fig. 2 the annealed sample scatters strongly at low Q-values with a Q^{-4} power law. According to Porod [23] this arises from particles with a sharp interface and the total interfacial area S per unit volume can be calculated from the corresponding Porod Law

$$\frac{d\Sigma}{d\Omega}\cdot Q^4 = 2\pi S(\Delta\rho_{\text{part}})^2. \tag{12}$$

Assuming that the particles are oxides and using a corresponding range of contrast values $\Delta\rho_{\text{part}}$ yields $S = 10^2-10^3$ cm^2/cm^3. As the Porod law is valid for $Q>5\cdot10^{-3}$ Å^{-1} the average radii of the scattering particles have to be larger than 20 nm. This leads to an approximate particle density of 10^{12} to 10^{13} cm^{-3} which is too low for detecting the particles by TEM. The upper limit of the particle density corresponds to about $1.5\cdot10^{-4}$ atomic fraction of oxygen for an average molar volume of oxides being about 15 cm^3/Mol-O. The "particles" may as well be voids formed by vacancy condensation. The estimation shows that even a small fraction of particles gives rise to strong Porod scattering at low Q-values. In one experiment we used a single crystal of Pd with a purity of 99.99%. However, the reduction of the Porod scattering was small.

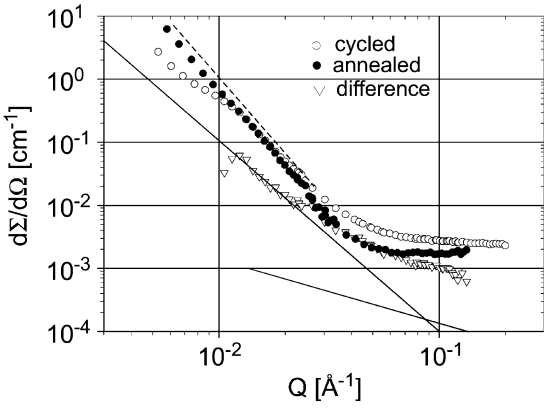

Fig. 2. Macroscopic scattering cross section for the annealed sample (closed circles) and the cycled sample (open circles). The dashed line has a slope of -4 and exemplifies the strong Porod scattering of the annealed and cycled samples at low Q. The steep straight line is the expected contribution from edge dislocations of a density of $2\cdot10^{11}$ cm^{-2} (cf. equation 6). The contribution from the core (cf. equation 5 with $r_c = b = 0.275$ nm and $\Delta V/V = 0.5$) corresponds to the straight line of slope -1. Triangles are the difference between cycled and annealed sample (values for $Q<2\cdot10^{-2}$ Å^{-1} are negative)

Internal deformation by cycling through the β-phase decreases the cross section at low Q and increases it at high Q (cf. Fig. 2). The decrease may be due to a partial annihilation of voids or oxides by the deformation process, whereas the increase may arise from the dislocations themselves. The increase presented in Fig. 2 was the largest one observed. In other cases it was less than the statistical error of the data. For a dislocation density of $2\cdot10^{11}$ cm^{-2} the contribution from both the core according to equation 5 and the strain field according to equation 6 are small indeed as shown in Fig. 2, even for favorable values of $r_c = b = 0.275$ nm and $\Delta V/V = 0.5$. Therefore, we do not expect the bare dislocations to contribute significantly to the measured cross sections. This is also true for the mixed term discussed before.

4.2. Hydrogen data

The total cross sections of a cycled sample doped with 0.84 and 1.05% H/Pd respectively are compared with the same cycled but hydrogen free sample in Fig. 3 after the incoherent scattering of hydrogen has been subtracted. The latter corresponds to $(d\Sigma/d\Omega)_{\text{inc}} = 4.345\cdot10-3\cdot c_H$ cm^{-1}, where c_H is the hydrogen concentration in % H/Pd. It can be seen that doping with hydrogen caused a remarkable increase of the cross section which has a Q^{-1}-dependence as expected from small angle scattering of line-type defects. The net scattering cross sections are presented in Fig. 4 for all the hydrogenated samples studied. The cross section increases with increasing H-content and within the Q-range of 0.02 to 0.1 Å^{-1} the Q^{-1} dependence is approximately fulfilled. For $Q<0.01$ Å^{-1} the

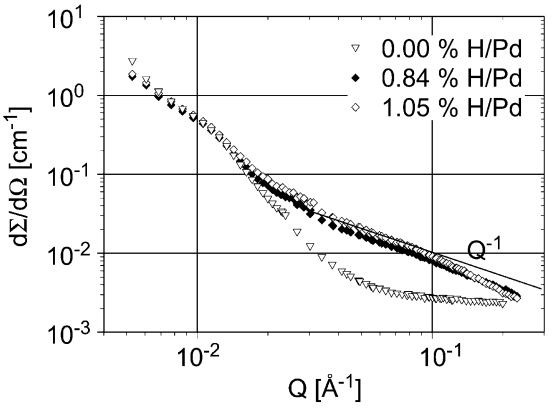

Fig. 3. Macroscopic scattering cross section of three cycled samples with different hydrogen concentrations (triangles: 0% H/Pd, full diamonds: 0.84% H/Pd and open diamonds: 1.05% H/Pd). Incoherent intensity of hydrogen is subtracted and the straight line has slope of -1.

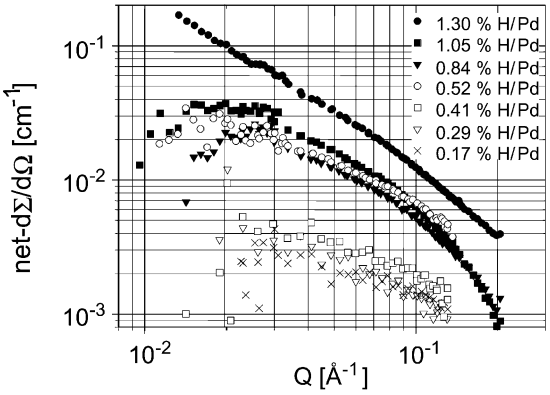

Fig. 4. Net scattering cross sections for hydrogenated samples which were cold-rolled and cycled before doping with H. Scattering of data points is due to measurement errors which are enhanced by calculating the net scattering cross section as a difference of two large quantities. The latter is especially true for low hydrogen concentrations.

net cross section even becomes negative. This will be discussed in connection with the deuterium results. For 1.3% H/Pd the behavior is slightly different, probably due to precipitation of the β-phase [6]. Deviations from the Q^{-1} dependence occur at large Q-values because of the exponential term in equation 8. In a modified Guinier plot of $\ln(Q \cdot d\Sigma/d\Omega)$ versus Q^2 a straight line is obtained as shown in Fig. 5 which has a slope of $R_0^2/4$. The agreement between experimental values and equation 8 as presented in Fig. 5 becomes worse for low hydrogen concentrations because of a decreasing signal to background ratio. Linear least square fits within the Q^2-range of 0.01 $Å^{-2}$ and 0.04 $Å^{-2}$ yield radii as presented in Table 1. The radius of the hydrogen cylinder is increasing with increasing hydrogen concentration within the α-phase. The intercept with the ordinate in Fig. 5 corresponds to $\ln(N_d \pi^3 H R_0^4 \Delta\rho^2)$ which was used to calculate the dislocation density $2N_dH$ as compiled in Table 1. On average, the dislocation densities are of the order of magnitude as the one determined from TEM micrographs.

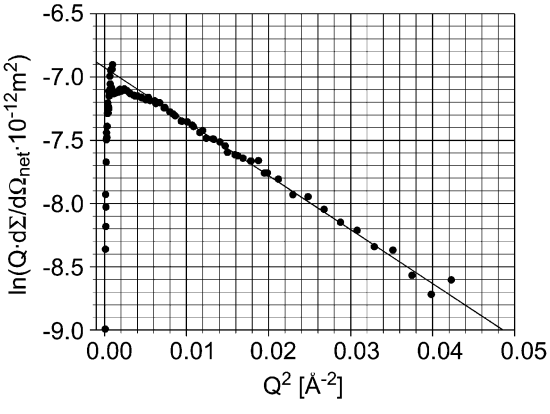

Fig. 5. Modified Guinier plot for the Pd-1.05% H sample. The slope of the straight line is $R_0^2/4$ yielding $R_0 = 13.1$ Å.

4.3. Deuterium data

The net cross sections for the deuterated samples is presented in Fig. 6. For D the solubility limit at room temperature is larger than for H [24] and, therefore, the 1.3% D/Pd sample is still within the α-phase. In contrast to the H-experiments, the samples were annealed before cycling and, therefore the dislocation density may be different. Overall, the behavior is similar to hydrogen despite an increasing net cross section at low Q-values. In addition the Guinier regime, i.e. the one where the exponential term in equation 8 affects the Q-dependence, is less pronounced, leading to smaller radii of about 4 Å in comparison with H at the highest concentration. This difference is diminished if a sample was used which was not annealed before cycling (cf. Fig. 7). In the latter case a radius of 10.8 Å is obtained. The deuterium data are not compiled in a table because they stem from samples of different origin. Nevertheless, all values for D are in agreement with values of 4–11 Å obtained by Heuser *et al.* for 0.55% D/Pd using different sample preparations [12, 13].

4.4. Direct comparison of H and D

During the experiments it turned out that the preparation of deformed samples was not reproducible unless samples were taken from the same stock annealed together in the same furnace and mounted in series within the same electrochemical cell for the cathodic and anodic cycling. Three samples treated this way were used for a direct comparison of H- and D-data. One was used for background measurements, one was doped with 0.8% H/Pd at 80°C by sorption from gaseous H_2, and the last one was doped the same way with D_2. The resulting net cross section is shown in Fig. 8. Over about one order of magnitude for the cross section the results follow a Q^{-1} dependence. A modified Guinier plot for hydrogen as the one in Figs 5 and 7 yields a radius of 6.5 Å. The curves shown in Fig. 8 were calculated with the aid of equations 8 and 10 using $R_0 = 6.5$ Å, a dislocation density of $2HN_d = 4.2 \cdot 10^{11}$ cm^{-2} and $f = 1.11$ (11% volume expansion).

Assuming the same radius for the hydride and deuteride cylinders and no volume expansion in the segregation zone ($f = 1$) leads to a ratio of cross sections (cf. equation 8) which is equivalent to the square of the ratio of scattering lengths, i.e. $(b_D/b_H)^2 = 3.18$. This is much larger than the experimentally observed ratio of 1.5 which can be explained by the volume expansion ($f = 1.11$) and the square of the corresponding scattering contrast given by equation 10.

One might also argue that the deviation from the expected ratio of cross sections arises from different radii for the two isotopes, with a less pronounced segregation of D to dislocations. As H and D have the same partial molar volume [25], the elastic interaction has to be the same. But as the terminal solubility of the α-phase is different for the isotopes [24: p. 1], it might be that the H-H interaction is more pronounced

Table 1. Cylinder radii as obtained from the modified Gunier analysis for different concentrations of the hydrogen. The radius increases within the α-Phase with the hydrogen concentration and reaches its maximum at the solubility limit (0.01 H/Pd). Using the intercept of a modified Guinier-plot $\ln(2N_d\pi^3HR_0^4\Delta\rho^2)$ the dislocation density is calculated. The increased H-concentration due to the presence of dislocations is calculated, too, and compared with experimental data (cf. Fig. 9)

c_H [10^{-2} H/Pd]	0.17	0.29	0.41	0.52	0.84	1.05
R [Å]	4.9±2	5.1±2	6.3±1.5	8.3±1.5	10.8±1.3	13.1±1
Dislocation density [10^{11} cm^{-2}]	$2.4\binom{-1.8}{+17}$	$2.0\binom{-1.5}{+13}$	$1.2\binom{-0.7}{+2.4}$	$1.5\binom{-0.7}{+1.8}$	$0.4\binom{-0.15}{+0.26}$	$0.8\binom{-0.2}{+0.8}$
Δc_H (experimental)		0.06	0.073	0.085	0.12	0.135
Δc_H (theoretical)		0.08	0.12	0.22	0.37	0.54

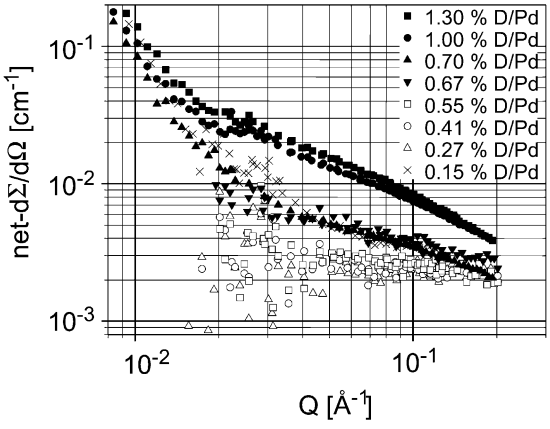

Fig. 6. Net scattering cross sections for deuterated samples which were annealed and cycled before doping with D. Scattering of data points is due to measurement errors which are enhanced by calculating the net scattering cross section as a difference of two large quantities. The latter is especially true for low deuterium concentrations.

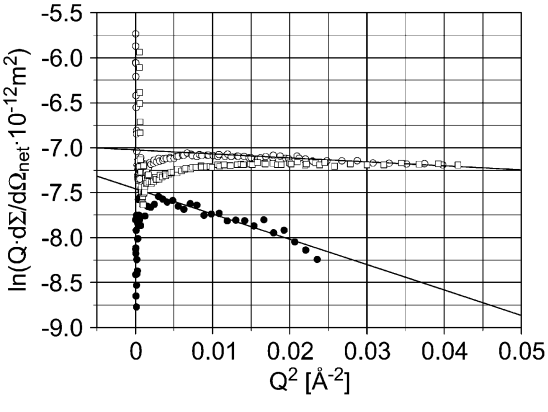

Fig. 7. Modified Guinier plot for an annealed and cycled sample (squares: 1.0% D/Pd and open circles: 1.3% D/Pd). A cold-rolled and cycled sample with 1.0% D/Pd (closed circles) is shown for comparison.

than the D-D one, leading to thicker cylinders for H. Under these circumstances the amount of trapped hydrogen should be larger for the same concentration of free isotopes far away from the dislocations. This will be discussed in the next section.

In Fig. 8 the deviations from the Q^{-1} dependence expected due to the exponential term in equation 8 are much more pronounced for H in comparison with

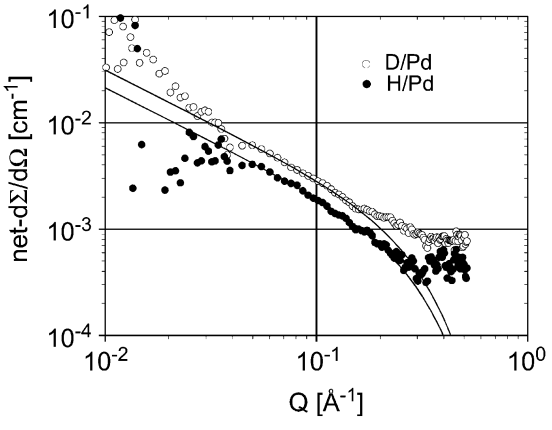

Fig. 8. Net scattering cross section of two annealed and cycled samples which were doped with 0.8% H/Pd (closed circles) and 0.8% D/Pd (open circles). The lines were calculated using equations 8–10 and with $R_0 = 6.5$ Å, a dislocation density of $2HN_d = 4.2\cdot10^{11}$ cm^{-2} and $f = 1.11$.

D, yielding a radius of $R_0 = 6.5$ Å for H if the data are evaluated in a modified Guinier plot (cf. Fig. 5). This is apparently the case for other deuterated samples as well (cf. Figs 5 and 7), although a direct comparison is difficult due to the different sample preparation. The discrepancy may arise because of an interference term between the isotopes and an unknown defect. Due to the different sign of the scattering length of the two isotopes its contribution would increase or decrease the net cross section. For low net cross sections, even a small interference term can change the results.

There is another interesting isotope effect for very low Q-values ($Q<4\cdot10^{-2}$ Å^{-1}). The cross section is decreased by doping with hydrogen, which leads to negative net cross sections, whereas deuterium increases the cross section. This effect also gives rise to the different deviations from the calculated curves as seen in Fig. 8. We interpret this as the contribution from a mixed term arising from the particles, causing Porod scattering and the isotopes. Then the different sign of b_D and b_H give rise to different signs of the mixed term.

4.5. Solubility enhancement for the two isotopes

The measured solubilities of H and D at 80°C in annealed and cycled Pd are presented in Fig. 9 in a double logarithmic plot. The slopes of the straight

lines are close to 2 in agreement with Sieverts' Law [6, 21] and the differences between H and D are well known to arise from different zero point energies in the solid for the two isotopes and different rotational entropies of the molecules in the gas phase [26: p. 10]. If the difference of isotope concentrations between deformed and annealed samples at a constant pressure is called Δc and the isotope concentration in the annealed sample being c_{free} then the concentration in the deformed sample far away from the dislocation will be c_{free}, too [6]. A plot of Δc versus c_{free} reveals no difference within the experimental error bars between the isotopes as shown in the inset of Fig. 9. Therefore, we can conclude that there seems to be no difference in the segregation of the two isotopes in agreement with previous measurements by Flanagan [27]. Thus the reduced difference between H- and D-SANS compared with the expectations from the scattering length has to be attributed to the volume expansion as discussed before.

5. DISCUSSION

5.1. Solubility enhancement and SANS

The solubility enhancement Δc as measured by an electrochemical technique has been used in a former study [11] to describe the interaction between hydrogen and dislocations in the framework of Statistical Mechanics. As a result diameters of hydrides formed at the dislocation were obtained which are in very good agreement with the ones obtained by SANS. For instance, a diameter of 28 Å was calculated at the solubility limit of 1% H/Pd which has to be compared with the value of 26 Å from Table 1. In the framework of elastic interaction alone, the extension of the segregated zone is much smaller [14], and therefore solute–solute interaction has to be taken into account.

A compilation of measured and calculated values of Δc is given in Table 1. With a dislocation density of $2 \cdot 10^{11}$ cm^{-2} and the radii from Table 1, the volume of the cylinders is calculated, and with the assumed local concentration of 0.6 (β-phase) the solubility enhancement Δc is obtained. Calculated and observed values have the same order of magnitude. The comparison has to be considered with caution because of (i) the different temperatures for the measurements of R_0 and Δc values, (ii) uncertainties with respect to the right value of the dislocation density (which is different for gas volumentry and SANS due to sample preparation) and (iii) experimental errors in the determination of R_0.

5.2. SANS radii as a function of H-content

Without stresses ($p = 0$) and for equilibrium between the hydride and saturated solid solution, the chemical potentials in the two phases have to be the same, i.e.

$$\mu_{(\text{hydride},p=0)} = \mu^0 + kT\ln c_{\text{ts}}, \tag{13}$$

where c_{ts} is the terminal solubility of hydrogen in Pd in equilibrium with the β-phase (of composition PdH_α). As the terminal solubility of H is 0.01 H/Pd at room temperature, the ideal solution approach for the configurational entropy (logarithmic term in equation 13) is justified. At the border between the cylindrical hydride and the solid solution a constant hydrostatic pressure p (cf. equation 2) is present, and the chemical potential is changed to

$$\mu = \mu^0 + kT\ln c_{\text{ts}} + pV_{\text{H}}. \tag{14}$$

Far away from the dislocation where hydrogen is free and where it has a local concentration of c_{f}, the chemical potential is given by

$$\mu = \mu^0 + kT\ln c_{\text{f}}. \tag{15}$$

Then equations 3 and 13 to 15 yield

$$c_{\text{f}} = c_{\text{ts}}\exp\left(-\frac{Gb(1+\nu)V_{\text{H}}}{6\pi(1-\nu)kTR}\right) = c_{\text{ts}}\exp\left(-\frac{C}{R}\right), \tag{16}$$

where C is 1.0 nm for edge dislocations of $b = 0.275$ nm in Pd. Besides c_{f}, the hydrogen trapped as a cylindrical hydride of composition α, radius R and length ρ_{d} contributes to the total concentration c_{tot}. Thus we have in terms of H/Pd

$$c_{\text{tot}} = \alpha\rho_{\text{d}}\pi R^2 + c_{\text{f}} = \alpha\rho_{\text{d}}\pi R^2 + c_{\text{ts}}\exp\left(-\frac{C}{R}\right). \tag{17}$$

If we use this implicit function of $R(c_{\text{tot}})$ and com-

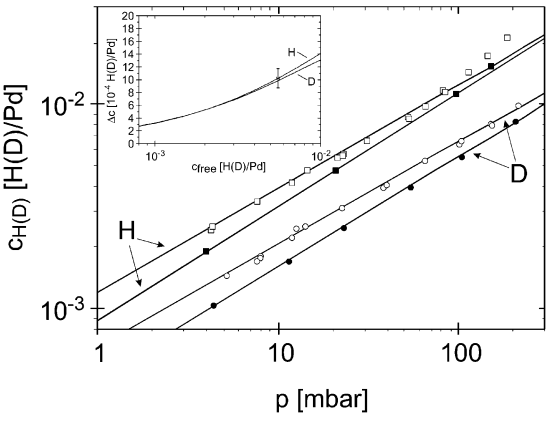

Fig. 9. Concentration of dissolved hydrogen and deuterium at 80°C as a function of partial pressure for annealed (open symbols) and cycled (closed symbols) samples. The straight lines are least square fits to the data points. The difference of concentrations Δc for annealed and cycled samples is segregated at the dislocations. Δc as calculated from the corresponding straight lines is plotted in the inset versus the concentration of free isotopes.

pare it in Fig. 10 with measured values, a good agreement is obtained by using a dislocation density of $2.2 \cdot 10^{11}$ cm^{-2}. The other quantities are $C = 1$ nm, $c_{ts} = 0.01$ H/Pd and $\alpha = 0.6$. This is considered to be additional evidence for an extended segregation of hydrogen, which requires taking into account both elastic and solute/solute interaction.

6. CONCLUSION

The combined approach of SANS and thermodynamic measurements leads to a consistent description of the interaction between hydrogen and dislocations as induced by elastic interaction and enhanced by solute–solute interaction. The formation of cylindrical "hydrides" along the dislocation line should give rise to large coherency stresses, which may relax by splitting a long cylinder into small ones and relaxing the compressive stresses in between by dislocation climb. Then the smaller length 2H of the cylinders should lead to deviations from the Q^{-1} dependence for $Q < (2H)^{-1}$. However, for periodically arranged cylinders, constructive interference should give rise to an additional peak at $Q \approx 2\pi/d$, where d is the distance of the smaller cylinders. Unfortunately Porod scattering at low Q-values and interference of this with hydrogen and deuterium scattering did not allow us to provide results for the length of cylinders. Obviously better samples would help to overcome these difficulties. Heuser *et al.* [12, 13] seemed to have better Pd-samples because they observed the expected deviations, although these were explained by a pronounced curvature of dislocations and a corresponding loss of correlation. However, the formula they derived [15] on the dependency of the cross section on H contains an error as shown in Appendix A.

The interpretation of data will be improved if better values for dislocation densities and the fraction of edge types are made available by careful X-ray diffraction measurements. The ultimate determination of H-segregation at dislocations may be possible in the near future by using the 3-dimensional atom probe, as done for boron in iron aluminide [10].

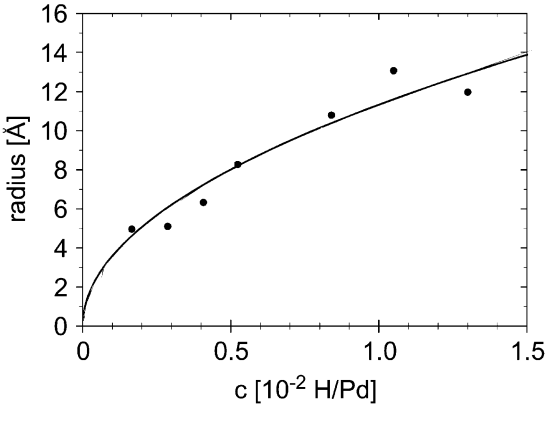

Fig. 10. Radius R_0 of the segregated hydride cylinder as a function of the total hydrogen concentration. The solid line was calculated from equation 17 with $C = 1$ nm, $c_{ts} = 0.01$ H/Pd, $\alpha = 0.6$, and $\rho_d = 2 \cdot 10^{11}$ cm^{-2}. The dislocation density was varied to obtain the best fit to the data.

Acknowledgements—The authors M.M. and R.K. are grateful for financial support provided by the Bundesministerium für Bildung und Forschnung (Project 03-KI5GOE). R.K. would like to thank J.J Rush at the NIST in Gaithersburg for supporting his stay. Helpful discussions with T. Udovic, J.J. Rush and D. Richter are acknowledged.

REFERENCES

1. Cottrell, A. H., in *Documents in Modern Physics*. Gordon Breach, New York, 1964.
2. Hirth, J. P. and Lothe, J., *Theorie of Dislocations*. McGraw-Hill, New York, 1968.
3. Cottrell, A. H. and Bilby, B. A., *Proc. Phys. Soc. London*, 1949, **A62**, 49.
4. Louat, N., *Proc. Phys. Soc., London*, 1956, **B69**, 459.
5. Beshers, D. N., *Acta metall.*, 1958, **6**, 521.
6. Kirchheim, R., *Progr. Mat. Sci.*, 1988, **32**, 262.
7. Neuhäuser, H. and Schwink, C., *Materials Science and Technology* Vol. 6. VCH, Weinheim, 1993.
8. Bouret, A. and Colliex, C., *Ultramicroscopy*, 1982, **9**, 183.
9. Xiao, S. Q. and Haasen, P., *Scripta Met*., 1989, **23**, 295 and 365
10. Blavette, D., Cadel, E., Fraczkiewicz, A. and Menand, A., *Science*, 1999, **286**, 2317.
11. Kirchheim, R., *Acta Met*., 1981, **29**, 835 and 845
12. Heuser, B. J., King, J. S., Summerfield, G. S., Boué, F. and Epperson, J. E., *Acta Metall. Mater*., 1991, **39**, 2815.
13. Heuser, B. J. and King, J. S., *J. Alloys Compounds*, 1997, **261**, 225.
14. Ross, D. K. and Stefanopoulus, K. L., *Z. Phys. Chem.*, 1994, **183**, 29.
15. Heuser, B. J., Ph.D.Thesis, University of Michigan, Ann Arbor, 1990.
16. Atkinson, H. H. and Hirsch, P. B., *Phil. Mag.*, 1958, **Ser. 8**, 213.
17. Haubold, A.-G., *IFF-Ferienkurs* (ISBN 3-89336-180-4), 1996, **27**, C6.21.
18. Baranowski, B., Majchrzak, S. and Flanagan, T. B., *J. Phys. F*., 1971, **1**, 258.
19. Sears, V. F., *Neutron News*, 1992, **3**, 26.
20. Jamieson, H. C., Weatherly, G. C. and Manchester, F. D., *J. Less Comm. Met*., 1976, **50**, 85.
21. Flanagan, T. B., Lynch, J. F., Clewley, J. D. and von Turkovich, B., *J. Less-Common Metals*, 1976, **49**, 13.
22. Anderton, C., Strither, N., Pote, J., Foley, R., Rebeiz, K., Nesbit, S. and Craft, A., *Scripta met.*, 1996, **35**, 1013.
23. Porod, G., in *Small-Angle X-ray Scattering*, ed. O. Glatter and O. Kratky. Academic Press, New York, 1983, 1983.
24. Lässer, R., *Tritium and Helium in Metals*. Springer Series in Materials Science, Springer, Berlin, 1989.
25. Peisl, H., in *Topics in Applied Physics* Vol. 28, ed. G. Alefeld and J. Völkl. Springer, Berlin, 1978, p. 53.
26. Fukai, Y., *The Metal–Hydrogen system*. Springer, Berlin, 1993.
27. Flanagan, T. B., *J. of the Korean Inst. of Metals*, 1987, **25**, 41.

APPENDIX A

In the following we repeat the derivation of equation 8 shortly, in order to extend the derivations given in textbooks by a term describing the dependence on the length of the cylinder $2H$. The coordi-

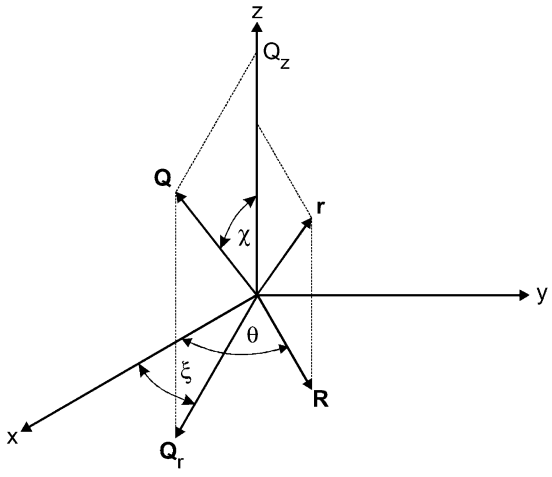

Fig. A1. Coordinates, vectors and angles used for the calculation of the scattering cross section.

nates used are shown in Fig. A1 and the macroscopic scattering cross section for N_d dislocations is

$$\frac{d\Sigma}{d\Omega} = N_d\langle AA*\rangle = N_d\langle\left|\int \Delta\rho(r,z,\theta)\exp(i\vec{Q}\vec{r})d^3\vec{r}\right|^2\rangle. \tag{A1}$$

The amplitude A is determined by using

$$\begin{aligned}\vec{Q}\vec{r} &= (\vec{Q}r + \vec{Q}_z)(\vec{z} + \vec{r}) \\ &= Qz\cos\chi + Q_r R\cos(\xi-\theta).\end{aligned} \tag{A2}$$

We evaluate the scattering amplitude for a cylinder of radius R_0 extending from $z = -H$ to $z = H$ first

$$\begin{aligned}A(Q) = \int_0^{R_0} RdR \int_0^{2\pi} d\theta \int_{-H}^{H} dz\Delta\rho \\ \exp[i(Qz\cos\chi + Q_r R\cos(\xi-\theta))].\end{aligned} \tag{A3}$$

Partial integration leads to

$$A(Q) = \frac{2\sin(HQ\cos(\chi))}{Q\cos\chi} \tag{A4}$$

$$\int_0^{R_0} RdR \int_0^{2\pi} d\theta\Delta\rho\exp[iQ_r R\cos(\xi-\theta))].$$

Expanding the exponential for $Q_r R \ll 1$ and using $\mu \equiv \cos\chi$ yields after integration

$$A(Q) = \frac{2F_0\Delta\rho\sin(HQ\mu)}{Q\mu}\left[1-\frac{1}{8}Q_r^2R_0^2\right]. \tag{A5}$$

The scattering cross section is obtained by averaging over all orientations of the dislocations

$$\begin{aligned}\frac{d\Sigma}{d\Omega} = \int_{-1}^{1} AA*d\mu = N_c\frac{4F_0^2\Delta\rho^2}{Q^2}\frac{1}{2\pi} \\ \frac{1}{2}\int_0^{2\pi} d\xi \int_{-1}^{1}\frac{\sin^2(HQ\mu)}{\mu^2}\left[1-\frac{1}{4}Q^2R_0^2(1-\mu^2)\right]d\mu\end{aligned} \tag{A6}$$

yielding

$$\begin{aligned}\frac{d\Sigma}{d\Omega} &= N_d\frac{2F_0^2\Delta\rho^2}{Q^2} \\ &\left\{\left[1-\frac{1}{4}Q^2R_0^2\right][-1 + \cos(2HQ) + 2HqSi(2HQ)]\right. \\ &\left. + \frac{1}{4}q^2R_0^2\left[1-\frac{\sin(2HQ)}{2HQ}\right]\right\},\end{aligned} \tag{A7}$$

where $Si(2HQ)$ is the sinus integral function. This result is different compared to the one derived in [15] and used in [12, 13], namely because the condition $QH \gg 1$ has to be used [23] in order to integrate equation 4.13 in [15] and, therefore, information about the scattering law for $QH \approx 1$ cannot be obtained. Equation A7 does not have this handicap and the expected result [23] for the cross section with Q approaching zero, i.e. for $QH \ll 1$ and $QR_0 \ll 1$ can be obtained

$$\frac{d\Sigma}{d\Omega} = N_d(2H\pi R_0^2)^2\Delta\rho^2. \tag{A8}$$

Finally equation 8 is retained from equation A7 with $QH \gg 1$ and $QR_0 \ll 1$ because of $2Si(\infty) = \pi$.